KfK 5254
Dezember 1993

Stress Intensity Factors and Weight Functions for Cracks in Front of Notches

T. Fett
Institut für Materialforschung

Kernforschungszentrum Karlsruhe

KERNFORSCHUNGSZENTRUM KARLSRUHE
Institut für Materialforschung

KfK 5254

Stress intensity factors and weight functions for cracks in front of notches

T. Fett

Kernforschungszentrum Karlsruhe GmbH, Karlsruhe

Kernforschungszentrum Karlsruhe GmbH
Postfach 3640, 76021 Karlsruhe

ISSN 0303-4003

Stress intensity factors and weight functions for cracks in front of notches

Abstract

The knowledge of stress intensity factors for cracks at notch roots is important for the fracture mechanical treatment of real components. Stress intensity factor solutions are available only for special notches and externally applied loads. For the treatment of more complex loadings as thermal stresses near the notch root the weight function is needed in addition.
In the first part of this report weight functions for cracks in front of internal notches are derived from stress intensity factor solutions under external loading available in the literature. The second part deals with cracks in front of edge notches. Limit cases of stress intensity factors are derived which allow to estimate stress intensity factors for cracks in front of internal elliptical notches with arbitrary aspect ratio of the ellipse and for external notches.

Spannungsintensitätsfaktoren und Gewichtsfunktionen für Risse an Kerben

Kurzfassung

Die Kenntnis der Spannungsintensitätsfaktoren für Risse an Kerben hat große Bedeutung für die bruchmechanische Behandlung realer Bauteile. Spannungsintensitätsfaktoren sind für einige Kerbtypen bei äußerer Belastung verfügbar. Für die Bewertung komplexerer Spannungen, z.B. thermische Spannungen vor der Kerbe, ist die Kenntnis der bruchmechanischen Gewichtsfunktion erforderlich.
Im ersten Teil des Berichts wird die Gewichtsfunktion für den Riß an einer elliptischen Innenkerbe aus Spannungsintensitätsfaktoren aus der Literatur berechnet. Der zweite Teil befaßt sich mit der einseitigen Außenkerbe. Lösungen einfacher Grenzfälle werden angegeben und es wird eine Interpolationsmethode vorgestellt, die es gestattet, beliebige dazwischenliegende Fälle zu behandeln.

Contents

1. Introduction

Under externally applied loads notches are enhancing stress. Therefore, cracks emanating from the notch root are of special interest in general fracture mechanics. Stress intensity factor solutions are available in the literature for externally applied tensile and bending loads [1]-[6]. In many cases, the stress in front of a notch is not caused by external forces. Such cases are for example:

- Crack surfaces directly loaded by internal pressure (pipes, vessels),
- cracks influenced by thermal stresses near the notch root,
- cracks in coarse-grained ceramics with crack-surface interaction.

The weight function method is an appropriate procedure for the computation of related stress intensity factors under such special loadings.
In the first part of this report weight functions for cracks in front of internal notches are derived from stress intensity factor solutions under external loading available in the literature. The second part deals with cracks in front of edge notches. The stress intensity factors under external load as well as under constant surface loading are determined with the Boundary-Collocation Method (BCM).
Limit cases of stress intensity factors will be derived which represent the behaviour of cracks in front of internal notches if the cracks are very long and very short compared with the notch-root radius. Based on these limit cases, an interpolation procedure is described which allows to estimate stress intensity factors for cracks in front of internal elliptical notches with arbitrary aspect ratio of the ellipse.
Estimation procedures on the basis of limit cases will also be presented for external notches.

2. Internal notches

2.1 Stresses at elliptical notches

2.1.1 Stresses at elliptical notches in infinite bodies

The stresses in front of internal notches are available only in cases with simple geometries and mechanics. This is true for elliptical notches in infinite bodies, where the problem has been solved by Muskelishvili ([7]) yielding the complex stress functions which satisfy the biharmonic differential equation and the boundary conditions.

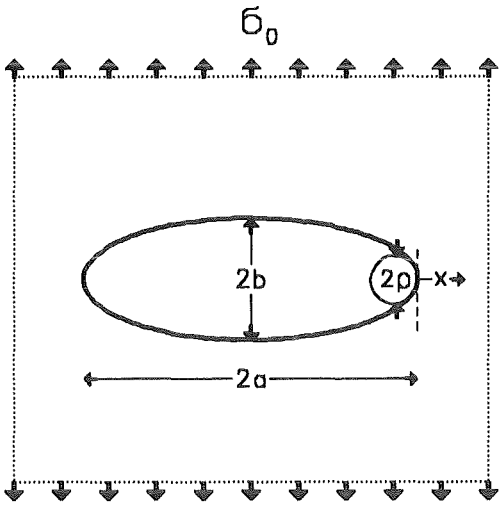

Figure 1. . Elliptical notch in an infinite body under remote tensile stresses σ_0.

Taking into account that any solution of the biharmonic equation can be expressed by two analytic functions of the complex variable z, the stresses in rectangular coordinates can be written as

$$\sigma_y + \sigma_x = 2\left[\varphi'(z) + \overline{\varphi'(z)}\right] = 4\,Re[\varphi'(z)] \tag{1}$$

$$\sigma_y - \sigma_x + 2i\tau_{xy} = 2\left[\bar{z}\varphi''(z) + \psi'(z)\right] \tag{2}$$

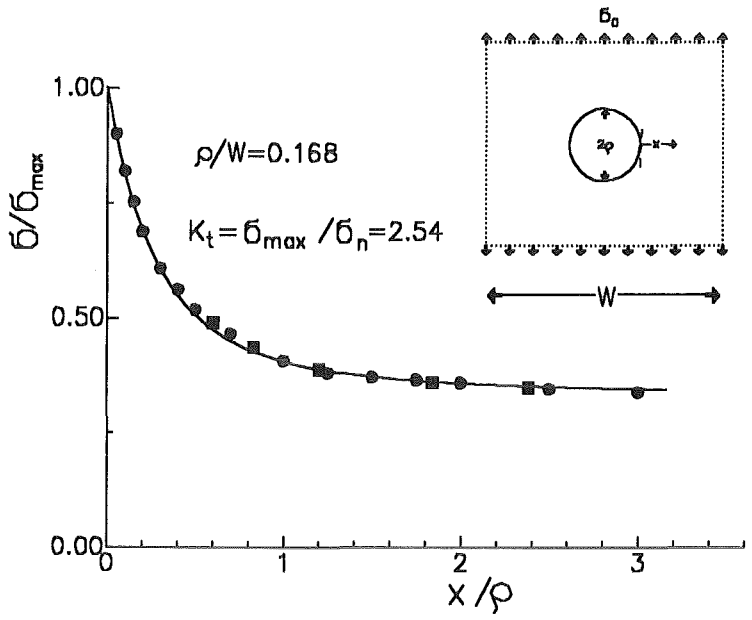

Figure 2. . Approximative stresses in front of a circular notch, compared with FE-results (circles: Armen et al. [10]) and experimental results (squares: Howland [11]).

The determination of the stresses is outlined in more detail in the Appendix. The following considerations will be restricted to the special case of stress distribution along the extended half-axis of the ellipse. The stress distribution at an elliptical notch under uniaxial remote tensile stress σ_0 results as ([8],[9])

$$(a-b)^2 \frac{\sigma_y}{\sigma_0} = b^2 + \frac{a|\kappa|}{\sqrt{\kappa^2 - a^2 + b^2}} \left[a - 2b + \frac{b^2(a-b)}{\kappa^2 - a^2 + b^2} \right] \tag{3}$$

$$(a-b)^2 \frac{\sigma_x}{\sigma_0} = -a^2 + \frac{a|\kappa|}{\sqrt{\kappa^2 - a^2 + b^2}} \left[a - \frac{b^2(a-b)}{\kappa^2 - a^2 + b^2} \right] \tag{4}$$

with $\kappa = x + a$. σ_y is the stress component perpendicular to the half-axis a and σ_x is the component in direction of the half-axis a, (fig.1). The notch root radius is given by

$$\rho = b^2/a \tag{5}$$

The maximum stress at $x = a$ is

$$\sigma_{y,max}/\sigma_0 = 2\sqrt{a/\rho} + 1 \tag{6}$$

In case of a notch with constant internal pressure $p < 0$ one obtains (see Appendix)

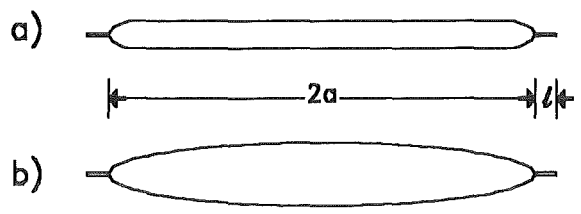

Figure 3. . A small crack in front of an internal notch.

$$\sigma_y = -p\,\frac{\lambda^4(1+m^2)+\lambda^2 m(m^2-6m+1)+2m^3}{(\lambda^2-m)^3} \qquad p<0$$

$$\lambda = \frac{x+a}{b+a} \pm \sqrt{\left(\frac{x+a}{b+a}\right)^2 - m} \tag{7}$$

$$b = \sqrt{a\rho} \quad , \quad m = \frac{\sqrt{a/\rho}-1}{\sqrt{a/\rho}+1}$$

with the maximum stress

$$\sigma_{y,max}/|p| = 2\sqrt{a/\rho} - 1 \tag{8}$$

In the special case of a circular notch ($m = 0$) with constant internal pressure it results from eq.(7)

$$\sigma_y = -\frac{p}{(x/\rho+1)^2} \tag{9}$$

2.1.2 An appropriate set-up for notch stresses in finite bodies

In order to extend the analytical solutions obtained for elliptical notches in infinite bodies we will use the similarity between narrow ellipses and cracks. Therefore, the notch stresses are transferred from the solution of the infinite body to the finite one by the ratio of the corresponding stress intensity factors according to

$$\sigma/\sigma_0 = \left(\frac{\sigma_{a/W\to\infty}}{\sigma_0} - 1\right)\frac{K}{K_{a/W\to\infty}} + C(a/W) \tag{10}$$

where the subscripts $a/W \to \infty$ are the solutions for the infinite body whilst the quantities for the finite body do not have subscripts. The correction term $C(a/W)$ is introduced to ensure the equilibrium of stresses.
The equilibrium condition can be expressed by

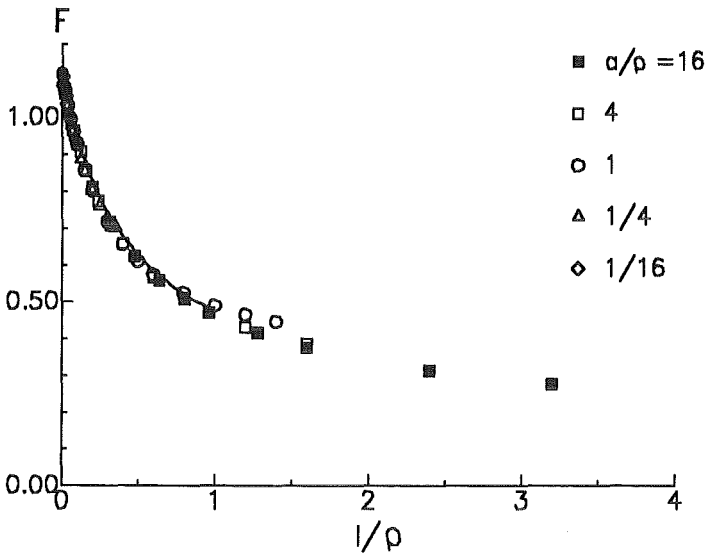

Figure 4. . Stress intensity factors for small cracks at a notch root (Newman [1]).

$$\frac{1}{W}\int_a^W \frac{\sigma}{\sigma_0}\, dx = 1 \tag{11}$$

yieding the function $C(a/W)$ as

$$C = \frac{W}{W-a} + \frac{K}{K_{a/W\to\infty}}\left[1 - \frac{1}{W-a}\int_a^W \frac{\sigma_{a/W\to\infty}}{\sigma_0}\, dx\right] \tag{12}$$

Several relations are normally used to describe the ratio $K/K_{a/W\to\infty}$. The simplest one is given by

$$K/K_{a/W\to\infty} = \sqrt{\sec\left(\frac{\pi}{2}\frac{a}{W}\right)} \tag{13}$$

2.1.3 Comparison with results from the literature

In order to compare the approximate stress distributions with results available, the circular notch in a finite body is considered. In the literature FE-calculations are reported by Armen et al. [10] and experiments were performed by Howland [11] (both references are quoted by Kujawski [5]). Figure 2 shows these results together with eq.(10) (solid line). The agreement is very good although the circular notch is very different from the case of a slender notch.

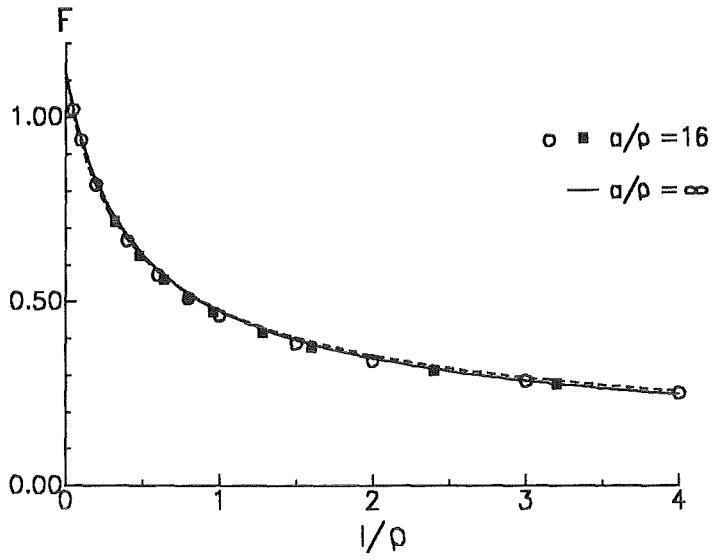

Figure 5. . Comparison of stress intensity factors for $a/\rho \gg 1$; symbols: $a/\rho = 16$ (squares: Newman [1]; circles: Nisitani and Isida, [13]); curves: solid line $a/\rho \to \infty$, dashed line eq.(15) (Lukas and Klesnil, [12]).

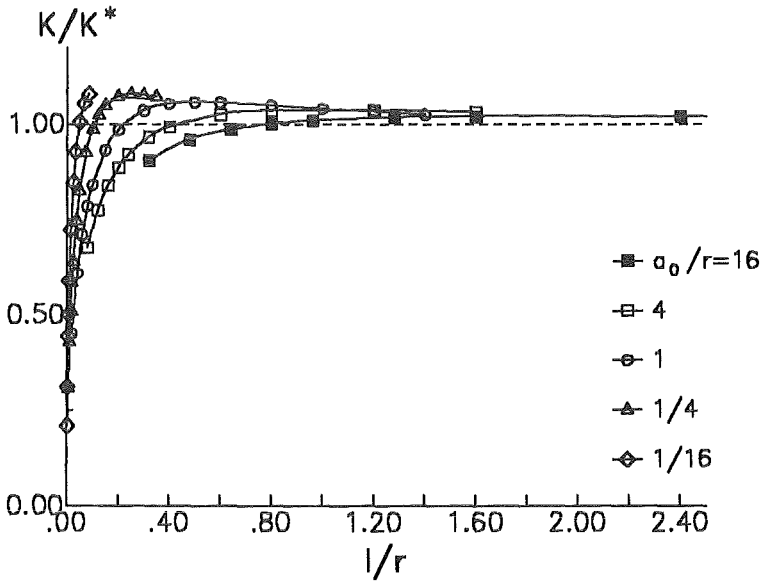

Figure 6. . Stress intensity factors for small cracks in front of elliptical notches normalised to the "long-crack" solution K^*.

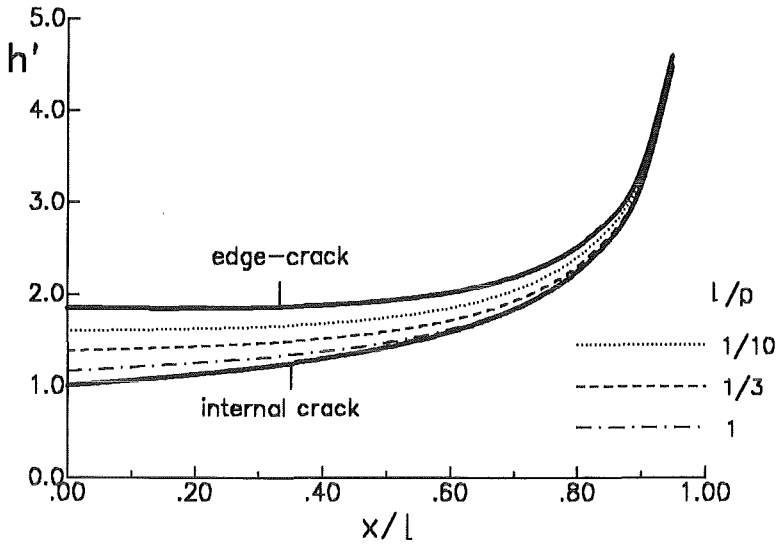

Figure 7. : Normalised weight function for cracks in front of an internal elliptical notch: $h' = h\sqrt{\pi\ell/2}$ for $a/\rho = 16$; solid lines: limit cases for edge-crack in a plate and internal crack in an infinite body.

2.2 Stress intensity factors for small cracks at the root of internal notches

A notch in an infinite body is shown in fig.3a. Its length is 2a and the notch radius is ρ. A small one-dimensional crack of length ℓ is placed at the notch root. The infinite body is loaded by a tensile stress σ_0. In order to allow analytical calculations to be made, the notch is replaced by a slender ellipse of the same length and the same radius ρ (fig.3b).
The stress intensity factor of the crack/notch-configuration may be written as

$$K_I = \sigma_0\left(1 + 2\sqrt{a/\rho}\right) F\sqrt{\pi\ell} \tag{14}$$

The geometric function F can be concluded from results of Newman [5] obtained with the Boundary Collocation method. In [1] stress intensity factors for cracks at the root of elliptical notches in an infinite body are given for values $a/\rho = 1/16, 1/4, 1, 4$, and 16. These data were also used in Schijve's [4] analysis.
The resulting geometric function is plotted in fig.4. It should be noted that for small values of ℓ/ρ the geometric function F is only dependent on ℓ/ρ and nearly independent of the ratio a/ρ.

In fig.5 the results of Newman for the narrowest ellipse ($a/\rho = 16$) are compared with results calculated by Nisitani and Isida [13] which were obtained for the same value a/ρ by parabolic interpolation of tabulated data (represented in [14]). The agreement is excellent. The solid line describes the solution for $a/\rho \to \infty$ given in (Nisitani and Isida [13]). There is obviously no significant deviation from the data resulting for $a/\rho = 16$. The additionally drawn dashed curve represents the guess of Lukas and Klesnil [12] which does not contain a/ρ:

$$F = \frac{1.1215}{\sqrt{1 + 4.5\ell/\rho}} \tag{15}$$

Their formula is in good agreement with the solution for $a/\rho \to \infty$ of Nisitani and Isida.

If we normalise the stress intensity factors described by eq.(14) to the stress intensity factors for long cracks $K^* = \sigma_0\sqrt{\pi(a_0 + \ell)}$, we observe the well-known behaviour of an "overshooting" of short-crack stress intensity factors over the long-crack values (fig.6).

2.3 Procedure for determination of the weight function

The weight function method developed by Bueckner [15] is an important procedure for the determination of stress intensity factors in case of complex stress distributions. For any given stress distribution $\sigma(x)$ in the uncracked component the stress intensity factor K_I results in

$$K_I = \int_0^\ell h_I(x, \ell)\sigma(x)\, dx \quad , \tag{16}$$

where h_I is the weight function. As shown by Rice [16], the weight function can be derived from CODs of a reference load case (subscript r) and the related reference stress intensity factor

$$h_I(x, \ell) = \frac{H}{K_{Ir}} \frac{\partial}{\partial \ell} v_r(x, \ell) \tag{17}$$

The modulus H is equal to the Young's modulus E for plane stress and $E/(1 - \nu^2)$ for plane strain, where ν is the Poisson ratio. Equation (17) has often been used as the basis for determination of approximate weight functions. The crack-opening displacements can be expressed by a power-series representation

$$v_r = \sum_{n=0}^{\infty} C_n \left(1 - \frac{x}{\ell}\right)^{n+1/2} \tag{18}$$

with the coefficients C_n dependent on the relative geometry. In order to determine the unknown coefficients of eq.(18), a number of conditions can be applied:

1. The crack-tip field is related to the stress intensity factor by (Petroski and Achenbach [17])

$$v_r(x \to \ell) = \left(\frac{8}{\pi}\right)^{1/2} \frac{K_{Ir}}{H} \sqrt{\ell - x} \tag{19}$$

2. The energy-balance condition requires ([17])

$$\int_0^\ell K_{Ir}^2 d\ell' = H \int_0^\ell \sigma_r(x) v_r(x, \ell) dx \tag{20}$$

3. As has been shown in ([18], [19]) for an edge crack, the second and third derivatives must vanish:

$$\frac{\partial^2 v}{\partial x^2} = 0 \quad , \qquad \frac{\partial^3 v}{\partial x^3} = 0 \quad , \quad \text{for } x = 0 \tag{21}$$

   This holds also for a crack perpendicular to a hole.
4. In order to fulfill the requirement of symmetry with respect to the center of the hole ($x = -a$), we can additionally introduce the condition

$$v' = 0 \quad \text{for} \quad x = -a \tag{22}$$

It may be recommended to use (20) for $\ell \ll a, \rho$ and (21) for $\ell \gg a, \rho$. In the intermediate range both conditions can be applied with variable weight.

This procedure and its modifications are well established in the literature and successfully applied in numerous investigations.

2.4 Results

In order to determine the weight function for the crack/notch-problem, the numerical results of Newman [1] and Nisitani and Isida [13] for $a/\rho \leq 1$ were chosen as the reference stress intensity factor and the stress distribution, eq.(3), as the reference stress σ_r. The weight function data resulting with the procedure described before are shown in fig.7 for the case $a/\rho = 16$ and several ratios ℓ/ρ. In addition, the two limit cases of an edge-crack in a plate ($\ell/\rho \to 0$) - using the solution derived in [20] - and an internal crack through the thickness of an infinite body ($\ell/\rho \to \infty$) are entered in fig.7. In case of a symmetrical crack/notch configuration (cracks at both sides of the notch) which has been considered in [1] and [13], the well-known formula for the weight function of a symmetrically loaded crack can be rewritten as

$$h_{int\ crack} = \frac{1}{\sqrt{\pi(\ell + a)}} \left(\sqrt{\frac{2a + \ell + x}{\ell - x}} + \sqrt{\frac{\ell - x}{2a + \ell + x}} \right) \tag{23}$$

In Tables Table 1-3 the weight function is given in the representation

$$h = \sqrt{\frac{2}{\pi \ell}} \frac{g(x/\ell, a/\rho)}{\sqrt{1 - x/\ell}} \tag{24}$$

which lends itself easily to interpolation. From a practical point of view, it is recommended to perform the interpolation with respect to the inverse parameter ρ/a or $\sqrt{\rho/a}$.
Weight functions for cracks in front of elliptical internal notches were determined with eqs.(18)-Glg. (23) The results are expressed by the function $g(x/\ell, \ell/\rho)$ according to eq.(24) and given in the following tables:

ℓ/ρ	$x/\ell = 0$	0.2	0.4	0.6	0.8	0.9	1.0
0.0	1.835	1.630	1.442	1.271	1.122	1.060	1.000
0.1	1.630	1.478	1.324	1.188	1.082	1.038	1.000
0.2	1.506	1.383	1.255	1.144	1.060	1.028	1.000
0.3	1.418	1.319	1.212	1.119	1.048	1.022	1.000
0.4	1.359	1.276	1.187	1.106	1.041	1.020	1.000
0.6	1.294	1.227	1.159	1.090	1.034	1.015	1.000
0.8	1.252	1.200	1.141	1.080	1.029	1.015	1.000
1.0	1.228	1.180	1.128	1.072	1.026	1.013	1.000

Table 1. Normalised weight function. $g(x/\ell, \ell/\rho)$ for $a/\rho = 1$.

ℓ/ρ	$x/\ell=0$	0.2	0.4	0.6	0.8	0.9	1.0
0.0	1.835	1.630	1.442	1.271	1.122	1.060	1.000
0.1	1.622	1.473	1.319	1.185	1.080	1.037	1.000
0.2	1.492	1.374	1.247	1.137	1.056	1.026	1.000
0.3	1.406	1.304	1.198	1.107	1.042	1.018	1.000
0.4	1.345	1.254	1.165	1.089	1.034	1.014	1.000
0.6	1.270	1.195	1.128	1.069	1.026	1.011	1.000
0.8	1.217	1.165	1.108	1.057	1.020	1.008	1.000
1.0	1.177	1.147	1.094	1.050	1.017	1.007	1.000

Table 2. Normalised weight function. $g(x/\ell, \ell/\rho)$ for $a/\rho = 4$.

ℓ/ρ	$x/\ell=0$	0.2	0.4	0.6	0.8	0.9	1.0
0.0	1.835	1.630	1.442	1.271	1.122	1.060	1.000
0.1	1.593	1.449	1.302	1.173	1.075	1.034	1.000
0.2	1.470	1.351	1.229	1.125	1.050	1.022	1.000
0.3	1.393	1.290	1.184	1.096	1.035	1.015	1.000
0.4	1.338	1.247	1.153	1.076	1.026	1.010	1.000
0.6	1.259	1.186	1.111	1.051	1.014	1.005	1.000
0.8	1.202	1.147	1.083	1.036	1.008	1.002	1.000
1.0	1.161	1.122	1.065	1.028	1.005	1.000	1.000

Table 3. Normalised weight function. $g(x/\ell, \ell/\rho)$ for $a/\rho = 16$.

2.5 Limit cases for stress intensity factors

Two limit cases for the stress intensity factor of small cracks in front of an elliptical notch can be identified (fig.8). The lower limit is given by an internal crack of total length $2(\ell + a)$ which is loaded by the stress distribution σ (eq.(3)) over the length ℓ. The limit stress intensity factor $K^{(1)}$ is

$$K^{(1)} = \int_0^{\ell} h_{int\ crack}\ \sigma\ dx \tag{25}$$

where $h_{int\ crack}$ is given by eq.(23). For small cracks ($\ell \ll \rho$) the situation of an edge crack is approached yielding the stress intensity factor $K^{(2)}$

$$K^{(2)} = \int_0^{\ell} h_{edge\ crack}\ \sigma\ dx \tag{26}$$

with the weight function $h_{edge\ crack}$ for an edge crack in a semi-infinite plate. Weight function solutions are given in the Appendix.

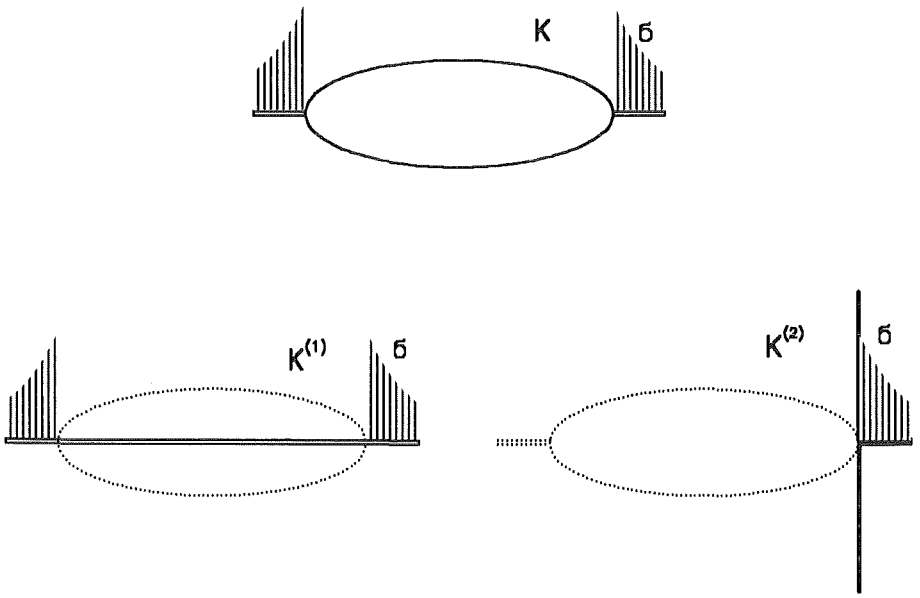

Figure 8. . Definition of the limit cases for stress intensity factors for a crack in front of an internal elliptical notch: $K^{(1)} < K < K^{(2)}$.

Figure 9 shows the limit cases $K^{(1)}$ and $K^{(2)}$ together with Newman's results for $a/\rho = 1$ and fig.10 illustrates an intercomparison for $a/\rho = 16$. The agreement between numerical data and the limit case $K^{(1)}$ is very good for $\ell/\rho > 1.5$. Therefore, the limit case $K^{(1)}$ is appropriate to represent the stress intensity factors for $\ell/\rho > 1.5$. This asymptotic agreement gives rise to an interpolation formula

$$K = \alpha K^{(2)} + (1 - \alpha) K^{(1)} \tag{27}$$

The interpolation factor α is plotted in fig.11 for $a/\rho = 1$ and $a/\rho = 16$ as a function of ℓ/ρ.
In order to characterise the notch-crack configuration we introduce a "view angle" ω as illustrated in fig.12. The crack-tip "sees" the notch under the total angle 2ω. The angle ω results from simple geometrical considerations and is given as the solution of the implicit equation

$$\frac{a}{b}\tan\omega\left[\frac{a}{b}\tan\omega - \left(1+\frac{\ell}{a}\right)\sqrt{1+\left(\frac{a}{b}\tan\omega\right)^2}\right] + 1 = 0 \tag{28}$$

In fig.13 the interpolation factor α is plotted versus ω. The resulting dependency can be approximated by the simple expression

$$\alpha \simeq \sin^{7/2}\omega \tag{29}$$

which is introduced in fig.13 as solid line.

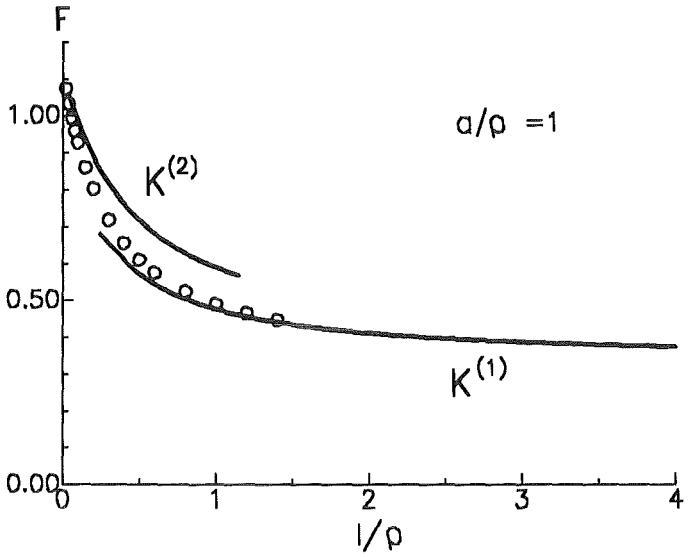

Figure 9. . Comparison of limit case solutions with numerical data of Newman [1] for $a/\rho = 1$.

2.6 Limit cases for the weight function

The comparison of the weight function data of fig.7 with the two limit cases gives rise to an interpolation factor β defined by

$$h = \beta h^{(2)} + (1 - \beta) h^{(1)} \tag{30}$$

where $h^{(2)}$ is the weight function for an edge crack (see Appendix) and $h^{(1)}$ is the value for an internal crack according to eq.(23). It becomes obvious from fig.7 that - in contrast to the interpolation factor α for stress intensity factors - β must also depend on x/ℓ. If we ignore this fact

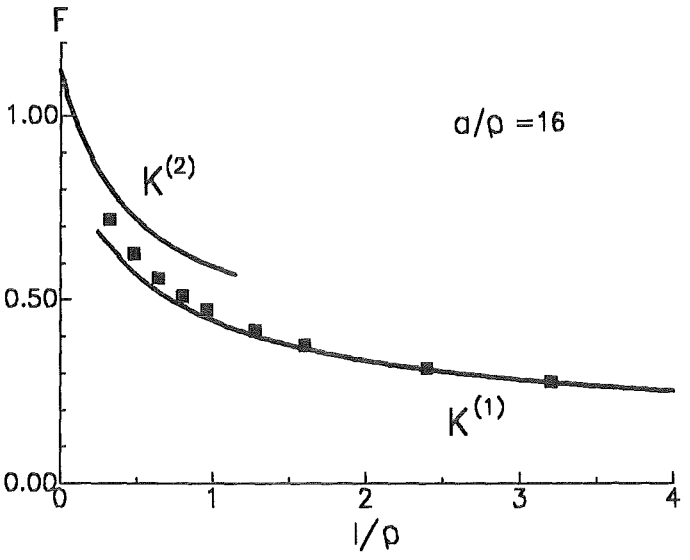

Figure 10. . Comparison of limit case solutions with numerical data of Newman [1] for $a/\rho = 16$.

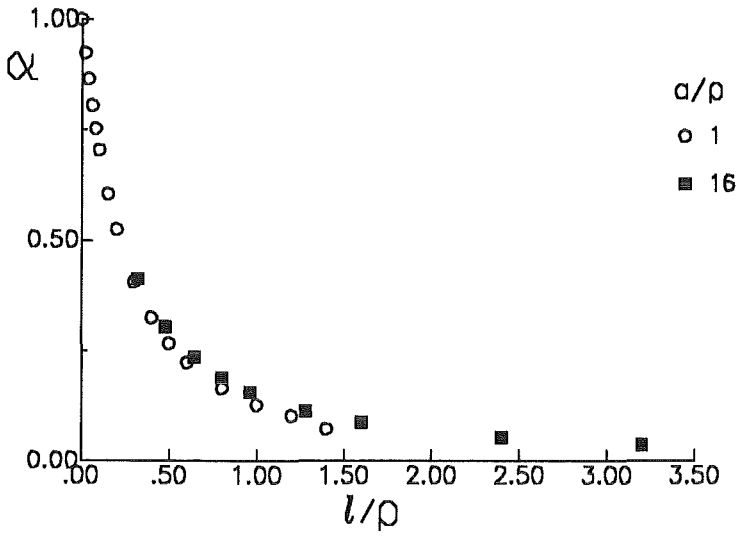

Figure 11. . Interpolation factor α defined by eq.(27) calculated on the basis of Newmans results.

and substitute α for β, we obtain the predicted weight functions as represented in fig.14. The comparison between the weight function of fig.7 and the interpolations of fig.14 shows that maximum deviations of about 3% occur. This accuracy is sufficient for most practical cases.

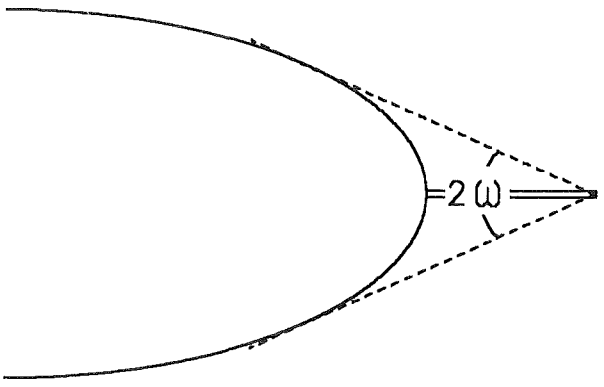

Figure 12. . Definition of the "view angle" ω.

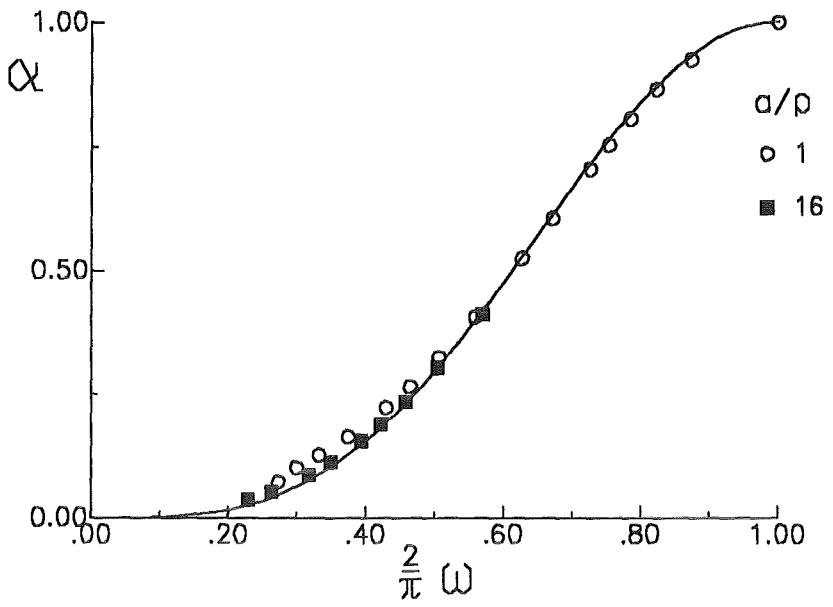

Figure 13. . Interpolation factor α as a function of the view angle ω.

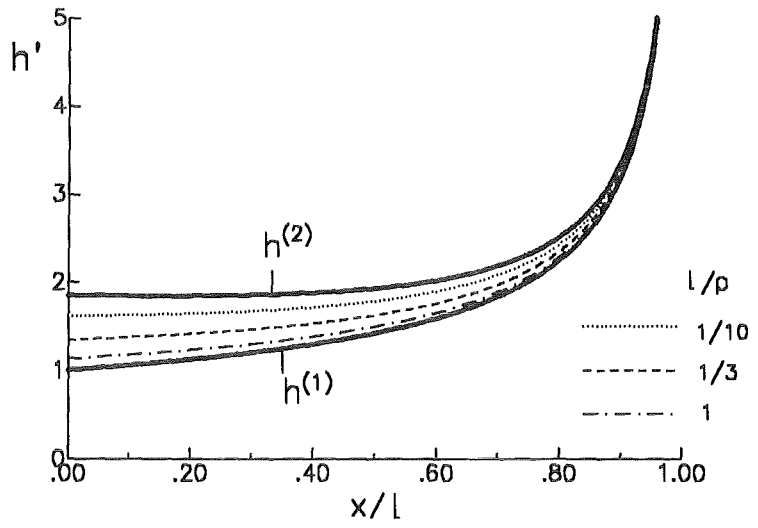

Figure 14. . Normalised weight function for cracks in front of an internal elliptical notch: $h' = h\sqrt{\pi\ell/2}$ for $a/\rho = 16$; solid lines: limit cases $h^{(1)}$, $h^{(2)}$; broken lines: interpolated with eq.(30) ($\beta = \alpha$).

3. External notches

An external notch in a body is shown in fig.15. Its length is a_0 and the notch width is $2d$. A small one-dimensional crack of length ℓ is placed at the notch root. Such notch-crack configurations are often used in fracture toughness testing of ceramic materials to approximate naturally sharp cracks. During the saw procedure small cracks are generated at the notch root. The real geometry of a saw-cut can be approximated by the two limit cases of a rectangular notch profile and a circular notch.

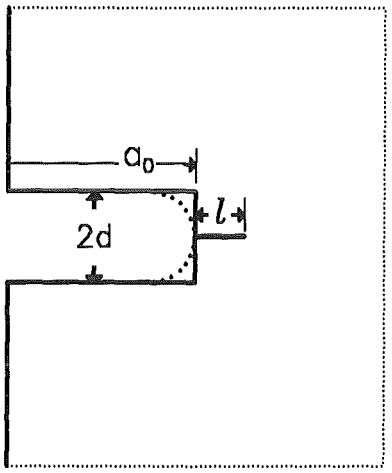

Figure 15. . A notch in a specimen with a small crack at the notch tip.

Notches prepared with thick saw blades tend more to adopt a rectangular shape and thin saw blades tend more to a circular shape. The two limit cases will be considered below. Calculations with the BCM were carried out with the geometric data $a_0/W = 0.5$ and $H/W = 1$. Figure 16 shows the location of the collocation points for the rectangular notch. Due to the symmetry with respect to $y = 0$, only the upper half of the specimen is considered. The Boundary Collocation procedure may be explained for the special case of the rectangular crack. The computation of stress intensity factors can be reduced to the determination of the stress distribution at the crack tip which is fully known if we succeed in determining the Airy stress function Φ. The stress components can be represented in polar coordinates - with the pole at the crack tip - expressed as

$$\sigma_r = \frac{1}{r}\frac{\partial \Phi}{\partial r} + \frac{1}{r^2}\frac{\partial^2 \Phi}{\partial \varphi^2}$$

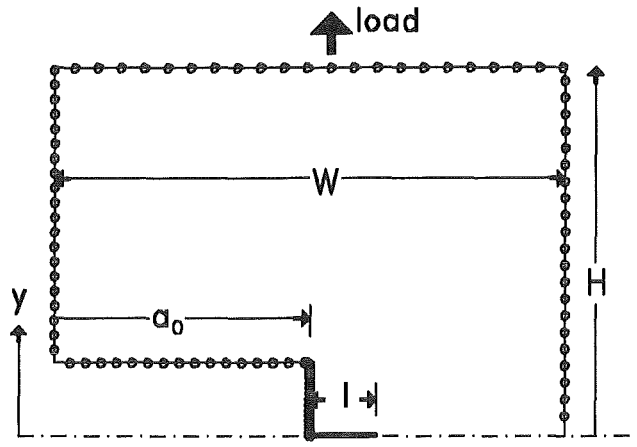

Figure 16. . Geometric data of the edge-notched specimen and distribution of the collocation points.

$$\sigma_\varphi = \frac{\partial^2 \Phi}{\partial r^2} \tag{31}$$

$$\tau_{r\varphi} = \frac{1}{r^2}\frac{\partial \Phi}{\partial \varphi} - \frac{1}{r}\frac{\partial^2 \Phi}{\partial r \partial \varphi}$$

The Airy stress function results as a solution of the bipotential equation

$$\Delta\Delta\Phi = 0 \tag{32}$$

The symmetrical part of the solution of eq.(32) - satisfying the condition of crack faces free of stress - is given in a series representation as

$$\Phi_s = \sum_{n=0}^{\infty} r^{n+3/2} A_n \left[\cos(n+3/2)\varphi - \frac{n+3/2}{n-1/2}\cos(n-1/2)\varphi \right]$$

$$+ \sum_{n=0}^{\infty} r^{n+2} A_n^* [\cos(n+2)\varphi - \cos n\varphi] \tag{33}$$

where the first sum accounts for singular stress distribution and the second for the regular portion. For practical application of eq.(33), the infinite series must be truncated after the Nth term for which an adequate value must be chosen ([21]).
Then the still unknown coefficients are determined by fitting the stresses (or the stress function) to the boundary conditions.

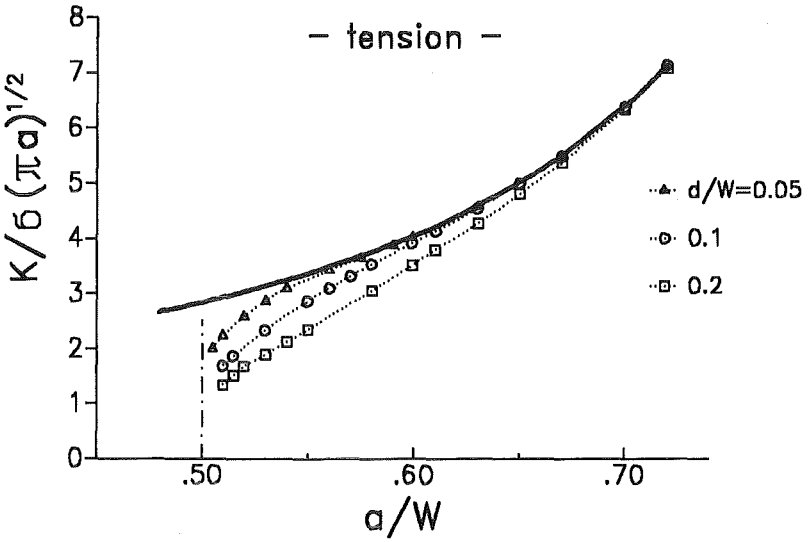

Figure 17. . Stress intensity factor for cracks at the tip of a rectangular notch under tensile load ($a_0/W = 0.5$).

3.1 The rectangular notch

The first practical example to be cited here ist the plate under **tensile** load. In this example the stresses at the border are

$$\sigma_x = 0 \quad \textit{for all perpendicular lines}, \qquad \tau_{xy} = \tau_{yx} = 0 \quad \textit{for the whole contour} \tag{34}$$

$$\sigma_y = \begin{cases} \sigma_0 & \text{for } y = H \\ 0 & \text{for } y = d \end{cases} \tag{35}$$

The boundary conditions for the stresses given by eq.(34) and (35) can be rewritten with reference to equivalent boundary conditions, which are applicable to the stress function Φ_s. The boundary conditions are

$$\frac{\partial \Phi_s}{\partial x}\Big|_{x=-a} = 0 \qquad \Phi_s|_{x=-a} = 0 \tag{36}$$

$$\frac{\partial \Phi_s}{\partial y}\Big|_{y=H} = 0 \qquad \Phi_s|_{y=H} = \sigma_0\left(\frac{x^2}{2} + ax + \frac{a^2}{2}\right) \tag{37}$$

$$\frac{\partial \Phi_s}{\partial x}\Big|_{x=W-a} = \sigma_0 W \qquad \Phi_s|_{x=W-a} = \frac{1}{2}\sigma_0 W^2 \tag{38}$$

For a selected number of N+1 collocation points a system of equations of type ((40) -(42)) with 2(N+1) unknowns results whose solution allows all 2(N+1) coefficients of eq.(33) to be determined. The expenditure in terms of computation can be reduced by selection of a rather large number of edge points and by solving subsequently the then overdetermined system of equations using the least squares of deviations. This gives a set of "best" coefficients. For the

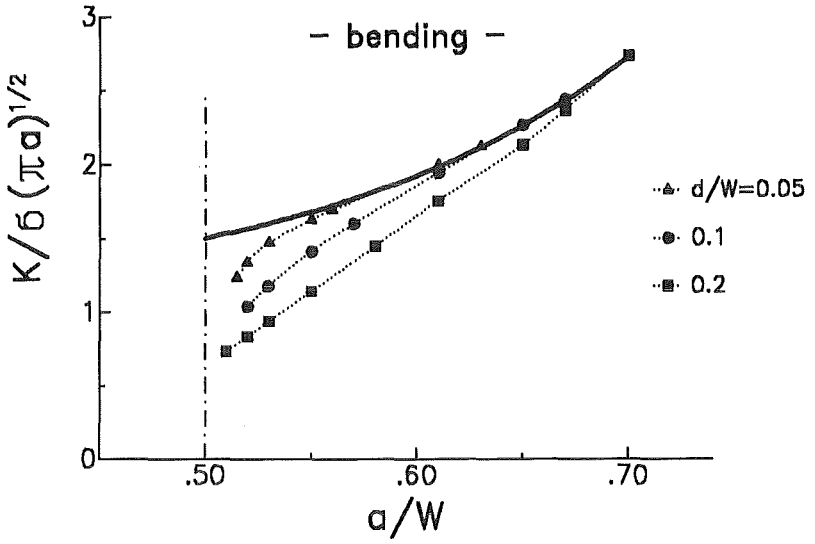

Figure 18. . Stress intensity factor for cracks at the tip of a rectangular notch under bending load ($a_0/W = 0.5$).

sake of simplicity, the stress σ_0 can be chosen arbitrarily to be $\sigma_0 = 1$. The stress intensity factor is given by the first coefficient of the series (33)

$$K_I = 3\sqrt{2\pi}\, A_0 \tag{39}$$

Figure 17 represents the resulting stress intensity factors for different values of the relative total crack length a/W and relative notch width d/W in a normalised representation. The solid line is the result for a crack of length $a_0 + \ell$ without notch obtained by the same Boundary Collocation procedure.

In case of a **bent plate** the boundary conditions have to be modified along the contour lines $y = H$ and $x = W - a$

$$\frac{\partial \Phi_s}{\partial y}\Big|_{y=H} = 0 \tag{40}$$

$$\Phi_s|_{y=H} = \sigma_0\left(-\frac{a^3}{3W} - \frac{a^2 x}{W} - \frac{a x^2}{W} - \frac{x^3}{3W} + \frac{x^2}{2} + ax + \frac{a^2}{2}\right) \tag{41}$$

$$\frac{\partial \Phi_s}{\partial x}\Big|_{x=W-a} = 0 \qquad \Phi_s|_{x=W-a} = \frac{1}{6}\sigma_0 W^2 \tag{42}$$

In fig.18 the stress intensity factors for the bending load case are plotted in the same way as in fig.17. Finally, fig.19 shows the ratio of the stress intensity factor for the notch/crack-configuration to the stress intensity factor K^* - representing a crack of the same total length under the same load

$$K_I^* = \sigma\sqrt{\pi a}\, F \tag{43}$$

(F = geometric function) - as a function of the ratio ℓ/d. The ratio of stress intensity factors attains the value $K_I/K^* = 1$ at about $\ell/d = 1$. This is independent of the load case chosen.

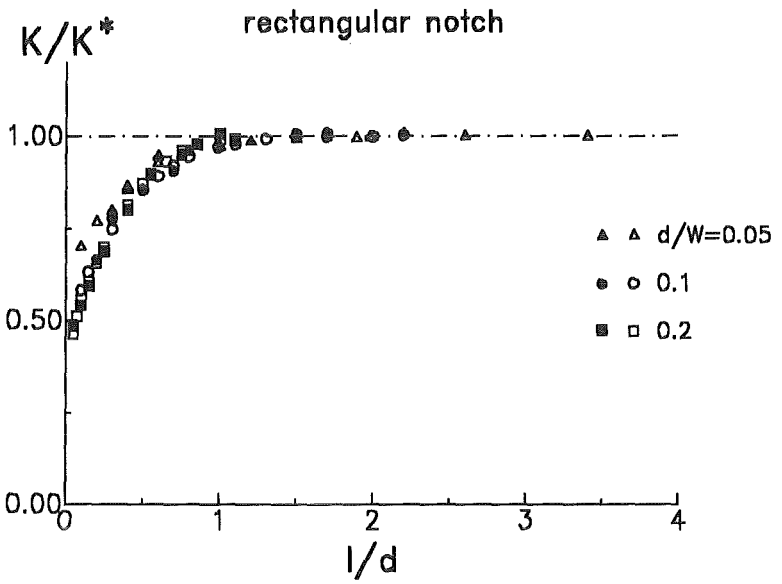

Figure 19. . Normalised stress intensity factors for cracks in front of a rectangular notch under tensile load (open symbols) and bending load (solid symbols) ($a_0/W = 0.5$).

3.2 The circular notch

In case of the circular notch root the boundary conditions along the circle are

$$\Phi_s|_{\rho=d} = 0 \quad , \quad \frac{\partial \Phi_s}{\partial \rho}|_{\rho=d} = 0 \tag{44}$$

where ρ is the radial coordinate with the origin in the centre of the circle.
The results for the circular notch are plotted in fig.20 (tension), fig.22 (bending) and in a normalised representation in fig.21.

The following consequences are obvious:

- The stress intensity factor of the crack/notch configuration increases monotonically with crack extension.
- The stress intensity factor for the crack of length $a_0 + \ell$ is an upper limit for the crack at the notch root. It is obvious that an "overshooting effect" as observed for cracks in front of internal elliptical notches (fig.6) can hardly be detected for the investigated geometries.
- For cracks with a length greater than the notch radius ($\ell > d$) the crack/notch configuration can be replaced by a crack of total length $a_0 + \ell$.
- For a semi-circular notch root the short-crack solution equals the long-crack solution earlier than for a rectangular notch.

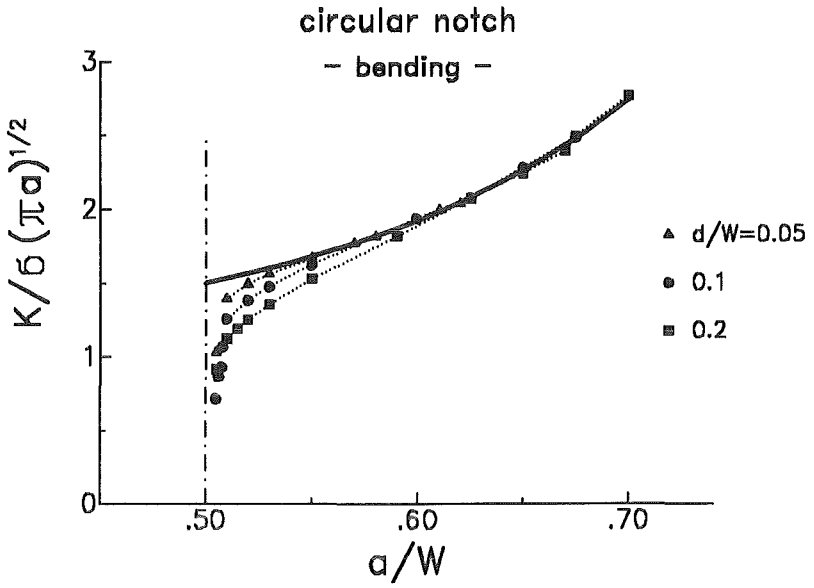

Figure 20. . Stress intensity factor for cracks at the tip of a semi-circular notch under tensile load ($a_0/W = 0.5$).

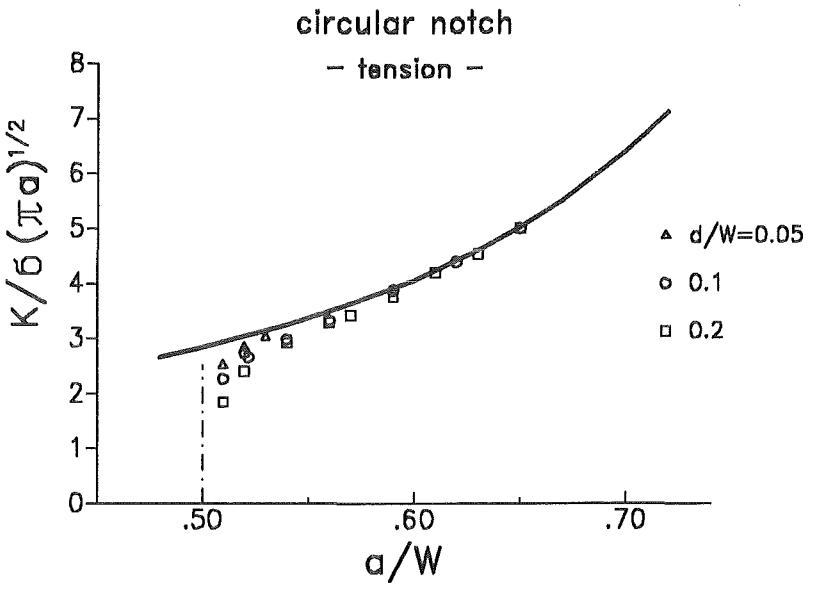

Figure 21. . Stress intensity factor for cracks at the tip of a semi-circular notch under bending load ($a_0/W = 0.5$).

The stress intensity factors for the circular notch (fig.21) can be expressed by

$$K/K^* \simeq \tanh\left(3\sqrt{\ell/d}\right) \tag{45}$$

for $a_0/W = 0.5$ and $0.05 \leq d/W \leq 0.2$. This dependency is entered in fig.23 as a solid curve.
Similar calculations as shown in detail in figs.20-23 for $a_0/W = 0.5$ were performed also for $a_0/W = 0.30$ and 0.70. The final results are represented in fig.24. The results obtained for the relatively wide notches investigated by BCM can be fitted as in eq.(45) by

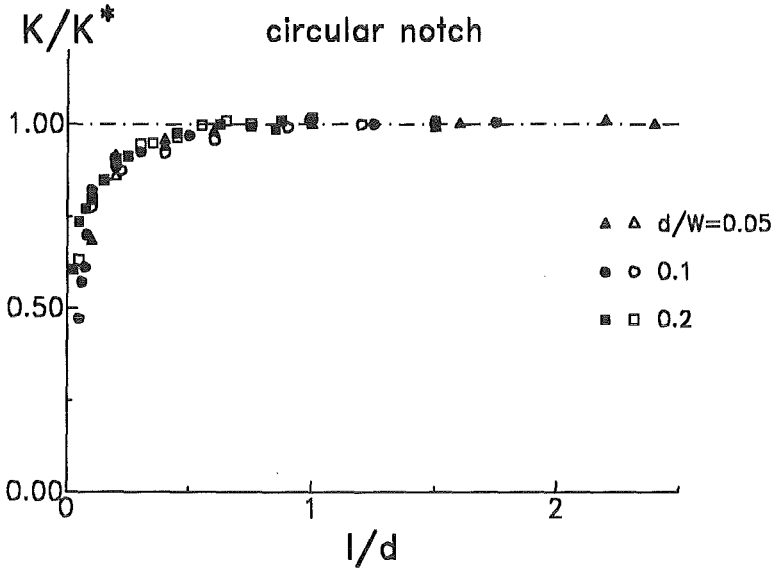

Figure 22. . Normalised stress intensity factors for cracks in front of a semi-circular notch under tensile load (open symbols) and bending load (solid symbols) ($a_0/W = 0.5$).

$$K/K^* = \tanh\left(\gamma\sqrt{\ell/d}\right) \tag{46}$$

with

$$\gamma \simeq \begin{cases} 3.7 & \text{for} \quad a_0/W = 0.3 \\ 3.0 & \text{for} \quad a_0/W = 0.5 \\ 2.3 & \text{for} \quad a_0/W = 0.7 \end{cases} \tag{47}$$

i.e. the value of γ decreases with the relative width d/a_0 of the notch. A theoretical lower limit of γ for $d/a_0 \to 0$ is $\gamma = 2.243$ which will be shown below.

3.3 Stress intensity factors for slender external notches

In case of very small cracks in front of a notch ($\ell/d \to 0$) the stress intensity factor is given by

$$K = \sigma_{max} 1.1215\sqrt{\pi\ell} \tag{48}$$

where σ_{max} is the maximum stress at the notch root. This maximum stress is available only for special notch problems. One of them is the slender notch with $d/a_0 \ll 1$.

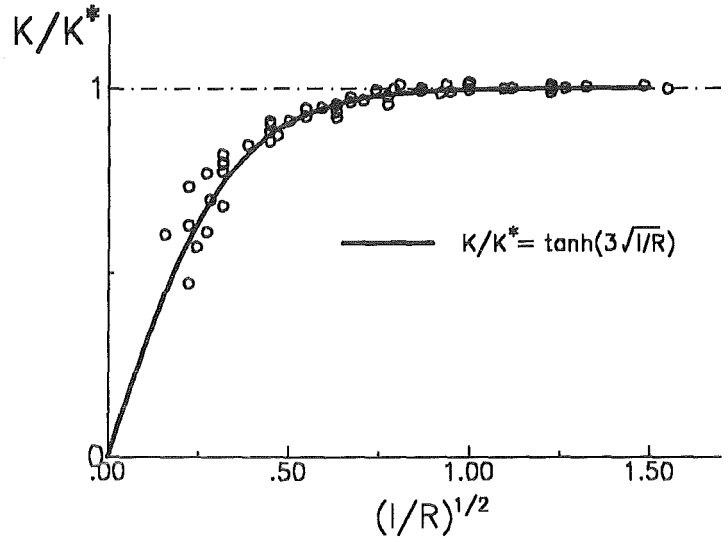

Figure 23. . Normalised stress intensity factors for cracks in front of a semi-circular notch ($R = d$).

3.3.1 Stresses in front of a slender edge notch

A simple possibility of determining the stresses in front of a slender notch is given by the procedure proposed by Creager and Paris [22] according to which the stresses in front of a slender notch of length a_0 and with the radius R can be derived from the stress intensity factor of a crack with the same length. Those authors calculated the stress distribution for arbitrarily loaded notches by use of the corresponding crack solution $K(a_0)$.

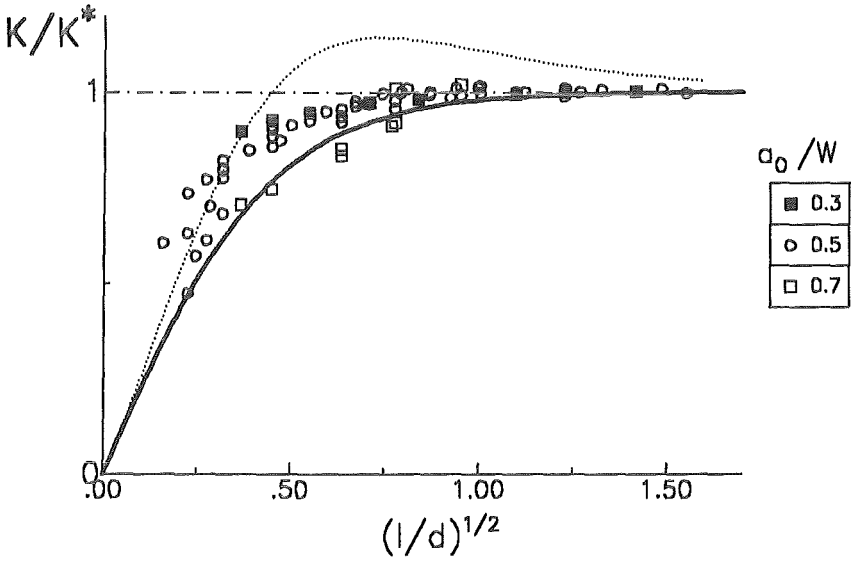

Figure 24. . Normalised stress intensity factors for cracks in front of a semi-circular notch ($R = d$); solid line: eq.(56), dotted line: eq.(58).

$$\sigma_y\Big|_{y=0} = \frac{K(a_0)}{\sqrt{\pi R z}}\left(1+\frac{1}{z}\right) \quad , \quad z = 1 + 2x/R \tag{49}$$

This relation describes fairly well the near-notch-tip behaviour of slender notches ($R/a \to 0$). Equation (49) is a good approximation of the stress field for $\ell/d < 1$. Additional terms for a higher order representation (which describes also the far stress field)

$$\sigma_y\Big|_{y=0} = \frac{K(a_0)}{\sqrt{\pi R z}}\left(1+\frac{C_1}{z}+\frac{C_2}{z^2}+\frac{1-C_1-C_2}{z^3}\right) \tag{50}$$

can be obtained from the equilibrium conditions

$$\int_{a_0}^{W} \sigma_y\, dx = \begin{cases} \sigma_0 W & \text{for tension} \\ 0 & \text{for bending} \end{cases} \tag{51}$$

and

$$\int_{a_0}^{W} \sigma_y\left(x-\frac{W}{2}\right) dx = \begin{cases} 0 & \text{for tension} \\ M_b & \text{for bending} \end{cases} \tag{52}$$

where M_b denotes the externally applied bending moment. For $\ell < d$ we can restrict the stress analysis to eq.(49). The maximum stress ($x = 0$) then results

$$\sigma_{max} = \frac{2K(a_0)}{\sqrt{\pi R}} \tag{53}$$

3.3.2 Stress intensity factors

The stress intensity factor for $\ell \ll R$ reads

$$K = 1.1215\sqrt{\ell/R}\; 2K(a_0) \tag{54}$$

Consequently, we obtain

$$K/K^* = 2.243\sqrt{\ell/R} \tag{55}$$

It is of importance that eq.(55) is independent of the type of the external load and is valid for tension as well as for bending. Taking into consideration the long-crack behaviour ($K/K^* \to 1$ for large ℓ/W) one may assume for the total dependency

$$K/K^* \simeq \tanh\left(2.243\sqrt{\ell/R}\right) \tag{56}$$

Equation (56) is additionally plotted in fig.24 as a solid line. Since in the special case of slender notches the two limit stress intensity factors are known, namely $K^{(1)}/K^* = 1$ and $K^{(2)}/K^*$ by eq.(55), one can check the applicability of the interpolation formula, eq.(27), for external notches with cylindrical notch root.
A simple geometrical consideration gives the "view angle"

$$\omega = \arcsin\left(\frac{d}{d+\ell}\right) \tag{57}$$

The prediction resulting from eqs.(27) and (29)

$$\frac{K_\omega}{K^*} = 1 - \frac{1 - 2.243\sqrt{\ell/d}}{(1+\ell/d)^{7/2}} \tag{58}$$

is plotted in fig.24 as dotted line. It is evident that the "overshooting effect" predicted by the interpolation procedure is in reality much less pronounced or even completely absent.
In this context, one should keep in mind that the stress distribution given by eq.(49) is only an approximative one.

3.4 Limit cases for stress intensity factors of cracks in front of external notches

Similar to the treatment applied for internal notches, also for external notches two limit stress intensity factors can be identified as illustrated in fig.25.

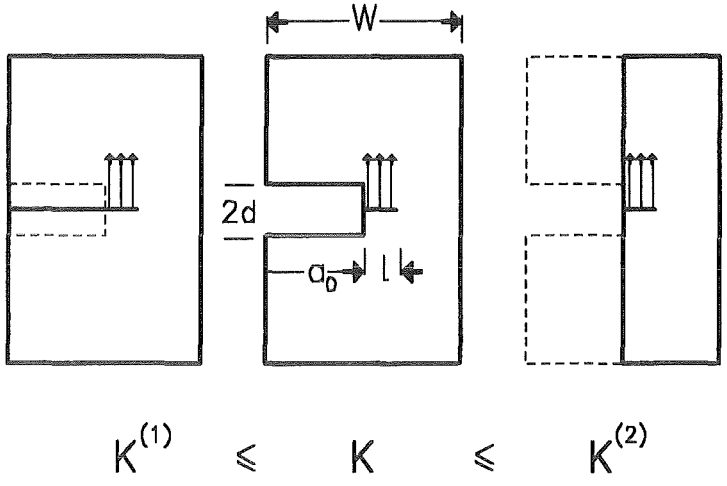

Figure 25. . Definition of the two limit stress intensity factors $K^{(1)}$ and $K^{(2)}$.

In fig.25 $K^{(1)}$ corresponds to the partially loaded edge crack of length $a_0 + \ell$ and $K^{(2)}$ is the stress intensity factor of an edge-crack of length ℓ in a body of reduced thickness W' ($W' = W - a_0$). Both limit cases are shown in fig.26 in terms of the geometric function F defined by

$$F = \frac{K}{\sigma\sqrt{\pi\ell}} \tag{59}$$

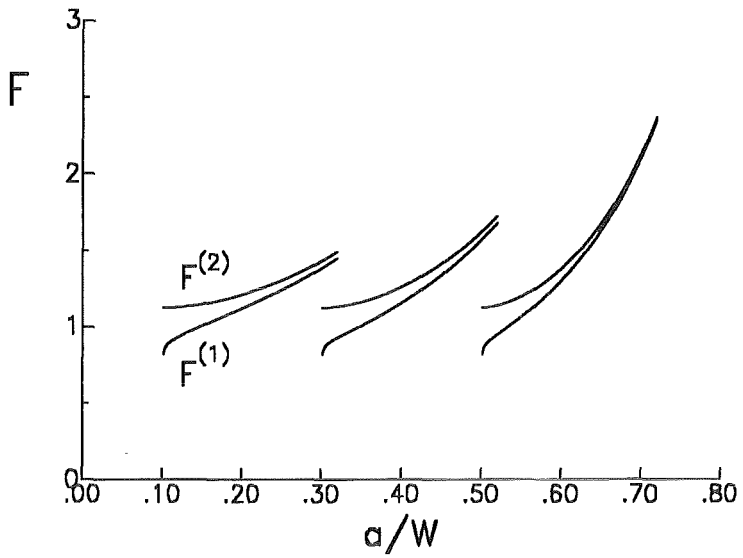

Figure 26. . Limit stress intensity factors $K^{(1)}$ and $K^{(2)}$ for different notch depths.

For first rough estimations it may be recommended to describe the stress intensity factor by the mean value of the limit case solutions resulting in deviations less than 10% for $\ell = a - a_0 > 0.02W$.
Figure 26 gives rise to introduction of an interpolation function α for edge notches, too. In order to decide whether or not the interpolation factor α determined for internal notches, eq.(27), is also appropriate under heavly deviating conditions, BCM-computations were performed for

- external notches with
- rectangular notch roots exposed to
- constant crack-surface loading.

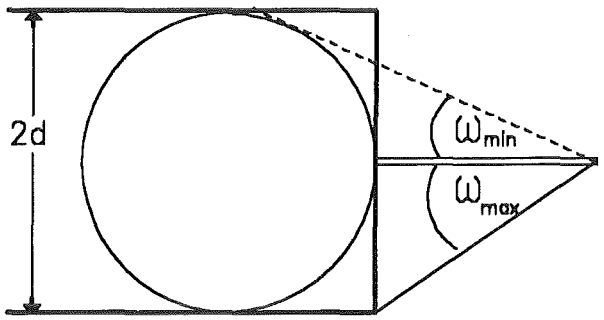

Figure 27. . Limit cases for the "view angle" ω in case of a rectangular edge notch.

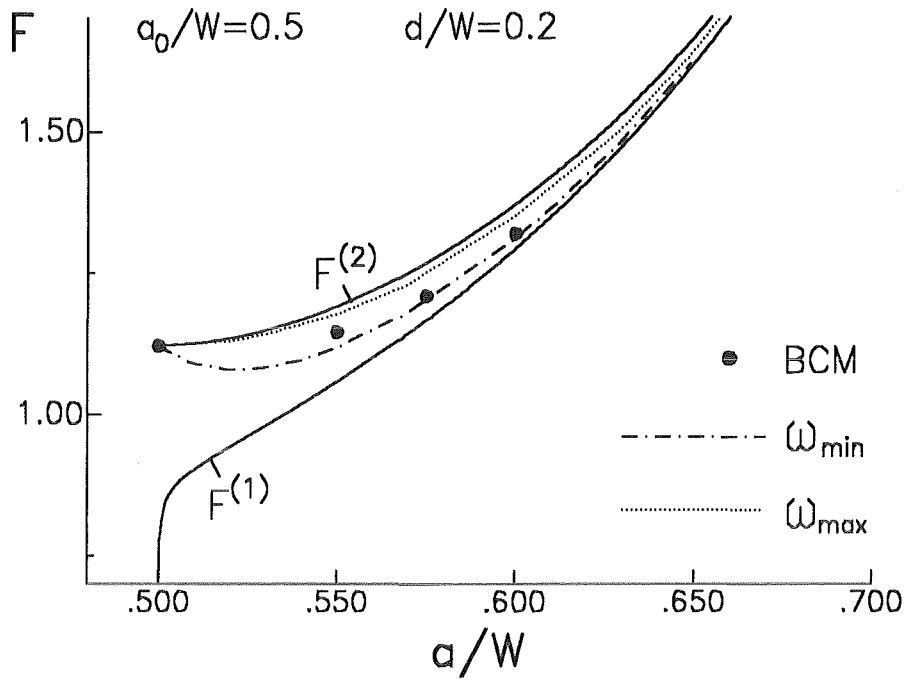

Figure 28. . Geometric function for cracks in front of external rectangular notches; symbols: determined with the Boundary Collocation Method, solid lines: limit cases; dotted and dash-dotted lines: interpolation of the limit stress intensity factors using eq.(29) for two extremal view angles.

Figure 29 shows the geometric function F, defined by eq.(59), for a rectangular edge notch with $a_0/W=0.5$ and $d/W=0.2$. The circles represent results obtained with the Boundary Collocation Method. The solid lines correspond to the limit cases $K^{(1)}, K^{(2)}$ and the dotted line is calculated

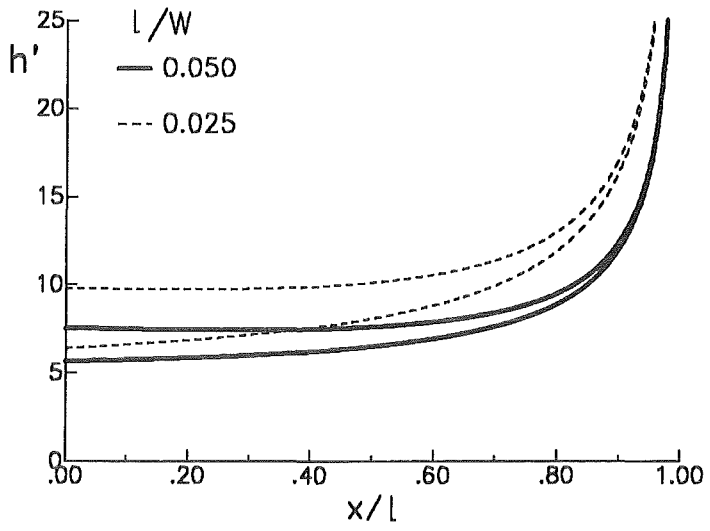

Figure 29. . Limit cases of weight functions ($h' = h\sqrt{\pi\ell/2}$) for small cracks in front of an external notch with $a_0/W = 0.5$ (upper curves: $h^{(2)}$, lower curves: $h^{(1)}$).

with the interpolation factor α according to eqs.(27) and (29). In section 2. the "view angle" ω was defined by the tangents from the crack tip to the ellipse of the notch. Since in the present case no ellipse is considered but a rectangular notch, we can introduce two extremal estimates for ω. In fig.27 the angle between the corners of the notch root is the maximum possible value, expressed as

$$\omega_{max} = arctan\left(\frac{d}{\ell}\right) \tag{60}$$

A minimum view angle is defined by the notch root radius $R = d$ of an elliptical notch of notch width d and its value is given by

$$\omega_{min} = arcsin\left(\frac{d}{d+\ell}\right) \tag{61}$$

The effective view angle is limited by

$$\omega_{min} < \omega < \omega_{max} \tag{62}$$

The results for the limit values ω_{min} and ω_{max} are also entered in fig.28. The agreement between predicted and numerically computed data is sufficient. The deviations between prediction and numerically determined stress intensity factors is less than 2%.

3.5 Weight function for cracks in front of external notches

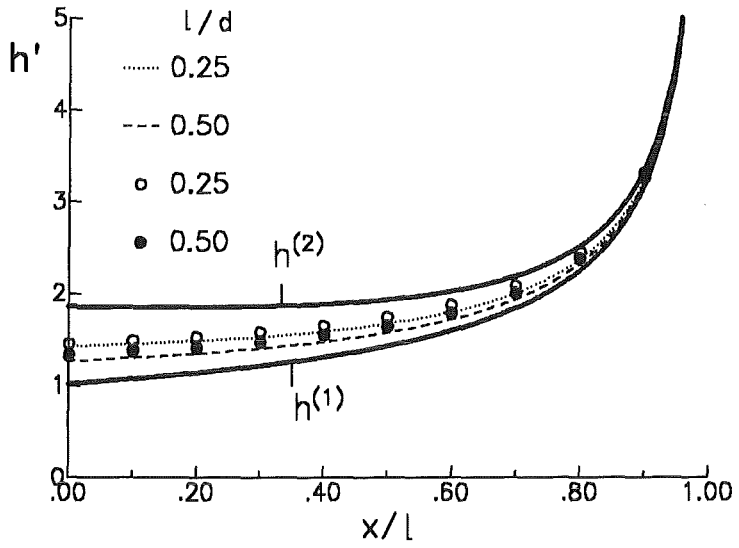

Figure 30. . Limit cases, interpolations and numerical weight functions for small cracks in front of an external notch ($a_0/W = 0.5$, $\ell/W = 0.0025$).

3.5.1 Limit cases

Similar to the treatment of cracks in front of internal notches the limit cases of the weight functions were also determined for cracks in front of external notches. The lower limit case of the weight function $h^{(1)}$ is identical with that of an edge crack of total length $a = a_0 + \ell$

$$h^{(1)} = h_{edge}\left(\frac{x + a_0}{\ell + a_0} , \frac{\ell + a_0}{W} \right) \tag{63}$$

The upper-limit case corresponds to an edge-crack of length ℓ in a body of reduced width $W' = W - a_0$

$$h^{(2)} = h_{edge}\left(\frac{x}{\ell} , \frac{\ell}{W - a_0} \right) \tag{64}$$

These two limit cases are plotted in fig.29 for $a_0/W = 0.5$ and $\ell/W = 0.1$ and 0.2. In fig.29 also the interpolated weight functions determined by

$$h = \alpha h^{(2)} + (1 - \alpha) h^{(1)} \quad , \quad \alpha = \sin^{7/2}(\omega) \tag{65}$$

and ω, defined by eq.(57), are entered.

3.5.2 Weight function for slender notches

In order to check the accuracy of the interpolation formula, the procedure of determination of the weight function from stress intensity factors described by eqs.(18)- (21) was applied to cracks in front of slender edge notches, too. For the stress intensity factor eq.(56) was used. In order to apply eqs.(18)- (21), the stress distribution in front of the notch root must be known. Also in this analysis, the stresses given by eq.(49) were used.
Numerically obtained weight functions for $\ell/R = 0.25$ and 0.5 are entered in fig.30 as symbols. The comparison between the numerical data and the interpolations of the limit cases (broken lines) shows maximum deviations of about 5%. These deviations should not be overrated since the stress distribution applied is only an approximation.

4. References

[1] J.C. Newman, An improved method of collocation for the stress analysis of cracked plates with various shaped boundaries, NASA TN D-6376 (1971).

[2] Y. Murakami, A method of stress intensity factor calculation for the crack emanating from an arbitrarily shaped hole or the crack in the vicinity of an arbitrarily shaped hole, Trans. Jap. Soc. Mech. Engrs. **44**(1978),423-32.

[3] H. Nisitani, M. Isida, Simple procedure for calculating K_I of a notch with a crack of arbitrary size and its application to non-propagating fatigue crack, Proc. Joint JSME-SESA (1982)150.

[4] J. Schijve, The stress intensity factor of small cracks at notches, Fatigue of Engng. Mater. and Struct. **5**(1982)77-90.

[5] D. Kujawski, Stress intensity factors for small cracks at notches, Fat. Fract. Engng. Mater. Struct. **14**(1991)953-65.

[6] G. Glinka, A. Newport, Universal features of elastic notch-tip stress fields, Int. J. Fatigue **9**(1987)143-150.

[7] N.I. Muskhelishvili, Some basic problems of mathematical theory of elasticity, Noordhoff 1953.

[8] J. Schijve, Stress gradients around notches, Report LR-297, University of Technology, Delft, 1980.

[9] D. Maugis, Stresses and displacements around cracks and elliptical cavities: Exact solutions, Engng. Fract. Mech. **43**(1992)217-255.

[10] H. Armen, A. Pifko, S. Levine, Finite element analysis of structures in the plastic range, NASA CR-1649(1971).

[11] R.C.J. Howland, On the stress in the neighborhood of a circular hole in a strip under tension, Trans. R. Soc. Ser.A **229**(1929/30)49-86, (quoted in [5]).

[12] P. Lukas, M. Klesnil, Fatigue limit of notched bodies, Mater. Sci. Engng. **34**(1978)61-66.

[13] H. Nisitani, Solutions of notched problems by body force method, in: Mechanics of Fracture (ed. by G.C. Sih), Vol.5 (1978), pp.1-68, Noordhoff, Leyden.

[14] Y.Murakami et al, Stress intensity factors handbook, Pergamon Press 1986.

[15] H. Bueckner, A novel principle for the computation of stress intensity factors, ZAMM **50**(1970),529-546.

[16] J. R. Rice, Int. J. Solids Structures **8**(1972)751-758

[17] H.J. Petroski, J.D. Achenbach, Engng. Fract. Mech. **10**(1978)257-66

[18] T. Fett, C. Mattheck, D. Munz, Engng. Fract. Mech. **27**(1987)697-715.

[19] T. Fett, Conditions for the determination of approximative COD-fields, Engng. Fract. Mech. **39**(1991),905-914.

[20] T. Fett, Stress intensity factors and weight functions for the edge cracked plate calculated by the Boundary Collocation Method, KfK-Report 4791, Kernforschungszentrum Karlsruhe, 1990.

[21] T. Fett, The stress intensity factor for small cracks at the root of a notch, Int. J. Fract. **54**(1992)R57-R64.

[22] M. Creager, P.C. Paris, Elastic field equations for blunt cracks with reference to stress corrosion cracking, Int. J. Fract. **3** 247-52 (1967).

5. Appendix

5.1 Stresses in front of elliptical internal notches

The stress distribution in front of an elliptical internal notch (Fig.1) can be computed from the complex potentials using the method of Muskelishvili [7]. The following considerations are restricted to the special case of the stress distribution along the extended half-axis ot the ellipse.
An elastical problem is completely solved if a function is found that satisfies the biharmonic differential equation and the boundary conditions. Taking into account that any solution of the biharmonic equation can be expressed by two analytic functions of the complex variable z, the stresses in rectangular coordinates can be written as

$$\begin{aligned} \sigma_y + \sigma_x &= 2\left[\varphi'(z) + \overline{\varphi'(z)}\right] = 4\,Re[\varphi'(z)] \\ \sigma_y - \sigma_x + 2i\tau_{xy} &= 2[\bar{z}\varphi''(z) + \psi'(z)] \end{aligned} \tag{66}$$

In order to determine the complex functions φ, ψ, it is of advantage to use the conformal mapping technique by introducing a new complex variable ζ and a mapping function $z = \omega(\zeta)$, which for elliptical geometries is given by

$$\begin{aligned} z = \omega(\zeta) &= r\left(\zeta + \frac{m}{\zeta}\right) \\ (r > 0,\ \ 0 \le m < 1)\ ,\ \ \zeta &= \lambda \exp(i\theta) \end{aligned} \tag{67}$$

The boundary of the ellipse is described by $|\zeta| = 1$ and the half-axes are defined by

$$\begin{aligned} a = r(1+m)\ \ ,\ \ \ \ b &= r(1-m) \\ \{\rightarrow\ r = (a+b)/2\ ,\ m &= (a-b)/(a+b)\} \end{aligned} \tag{68}$$

The stresses are now expressed as

$$\begin{aligned} \sigma_y + \sigma_x &= 4\,Re\left[\frac{\varphi'(\zeta)}{\omega'(\zeta)}\right] \\ \sigma_y - \sigma_x + 2i\tau_{xy} &= 2\left[\frac{\overline{\omega(\zeta)}}{\omega'(\zeta)}\left[\varphi'(\zeta)/\omega'(\zeta)\right]' + \frac{\psi'(\zeta)}{\omega'(\zeta)}\right] \end{aligned} \tag{69}$$

The stress functions for the elliptical internal notch under constant pressure p_0 were determined by Muskhelishvili [7] as

$$\varphi(\zeta) = -\frac{p_0 rm}{\zeta} \quad , \quad \psi(\zeta) = -\frac{p_0 r}{\zeta} - \frac{p_0 rm}{\zeta}\frac{1+m\zeta^2}{\zeta^2 - m} \tag{70}$$

In [7] the special case of a slot ($m = 1$) was treated. The solution for arbitrary ellipses can be found by introducing eq.(70) into (69) with

$$\zeta = \lambda \exp(i\theta) = \lambda(\cos\theta + i \sin\theta) \tag{71}$$

and

$$\begin{aligned}
\omega &= r[(\lambda + m/\lambda)\cos\theta + (\lambda - m/\lambda)\, i \sin\theta] \\
\overline{\omega} &= r[(\lambda + m/\lambda)\cos\theta - (\lambda - m/\lambda)\, i \sin\theta] \\
\omega' &= r\left[1 - \frac{m}{\lambda^2}(\cos 2\theta - i \sin 2\theta)\right] \\
\overline{\omega'} &= r\left[1 - \frac{m}{\lambda^2}(\cos 2\theta + i \sin 2\theta)\right]
\end{aligned} \tag{72}$$

Especially for $\theta = 0$ (i.e. the extension of the half-axis) one obtains:

$$\begin{aligned}
\sigma_y + \sigma_x &= p_0 \frac{4m}{\lambda^2 - m} \\
\sigma_y - \sigma_x &= -2p_0(m-1)^2 \frac{\lambda^2(\lambda^2 + m)}{(\lambda^2 - m)^3}
\end{aligned} \tag{73}$$

Adding the two equations (73) and subtracting them yields the stress components σ_y, σ_x

$$\sigma_y = -p_0 \frac{\lambda^4(1+m^2) + \lambda^2 m(m^2 - 6m + 1) + 2m^3}{(\lambda^2 - m)^3} \tag{74}$$

$$\sigma_x = -p_0 \frac{\lambda^4(m^2 - 4m + 1) + \lambda^2 m(m+1)^2 - 2m^3}{(\lambda^2 - m)^3} \tag{75}$$

For the elliptical notch under uniaxial remote tension Muskhelishvili's stress functions are

$$\begin{aligned}
\varphi(\zeta) &= \frac{1}{4}\sigma_0 r\left(\zeta + \frac{2-m}{\zeta}\right) \\
\psi(\zeta) &= -\frac{1}{2}\sigma_0 r\left(\zeta + \frac{1}{m\zeta} - \frac{(1+m^2)(1-m)}{m}\frac{\zeta}{\zeta^2 - m}\right)
\end{aligned} \tag{76}$$

With these potential functions one obtains

$$\begin{aligned}
\sigma_y = \frac{\sigma_0}{2(\lambda^2 - m)^3}&\left[2\lambda^6 + \lambda^4(m^2 - 4m + 1)\right. \\
&\left. + \lambda^2(m^3 - m^2 - 5m + 3) + m(m^2 + 2m - 1)\right]
\end{aligned} \tag{77}$$

$$\sigma_x = -\frac{\sigma_0}{2(\lambda^2 - m)^3} \cdot \tag{78}$$
$$\left[\lambda^4(m^2 - 2m - 3) + \lambda^2 m(m^2 + m + 3) + 3\lambda^2 - m(m^2 + 2m + 1)\right]$$

5.2 Weight function for the edge-cracked plate

A weight function for an edge-crack in a plate is [20]

$$h_l = \sqrt{\frac{2}{\pi a}} \frac{1}{\sqrt{1 - x/a}\,(1 - a/W)^{3/2}} \left[(1 - \frac{a}{W})^{3/2} + \sum C_{\nu\mu}(1 - x/a)^{\nu+1}(\frac{a}{W})^{\mu}\right] \tag{79}$$

with the coefficients $C_{\nu\mu}$

	$\mu=0$	1	2	3	4
$\nu=0$	0.4980	2.4463	0.0700	1.3187	-3.067
1	0.54165	-5.0806	24.3447	-32.7208	18.1214
2	-0.19277	2.55863	-12.6415	19.763	-10.9860

Table 4. . Coefficients for eq.(79).